43rd AIAA/ASME/SAE/ASEE Joint Propulsion Conference & Exhibit
8 - 11 July 2007, Cincinnati, OH

AIAA 2007-5305

Experimental and Numerical Examination of the BHT-200 Hall Thruster Plume

Michael R. Nakles*, Lubos Brieda*, and Garrett D. Reed*
ERC, Inc., Edwards Air Force Base, CA 93524

William A. Hargus, Jr.†
Air Force Research Laboratory, Edwards Air Force Base, CA 93524

Randy L. Spicer‡
Virginia Tech, Blacksburg, VA 24061

The plume of a Busek BHT-200 xenon Hall thruster has been characterized through measurements from various plasma electrostatic probes. Ion current flux, plasma potential, plasma density, and electron temperatures were measured in the near-field of the plume to 60 cm downstream of the exit plane. These experimentally derived measurements were compared to simulations of the thruster/vacuum chamber environment using the plasma plume code DRACO. The goals of this study were to gain understanding of the effect of the vacuum facility on the thruster plume and to determine the fidelity of the DRACO numerical simulation.

I. Introduction

THE Hall thruster is an electric thruster well suited for missions requiring low thrust, high specific impulse operations. Studies of the plume plasma properties are required to better understand both the thruster plume environment as well as the effect of ground testing facility limitations. This study examines the ion flux, plasma density, plasma potential, and electron temperature of the Busek BHT-200 laboratory Hall thruster from the near plume to 60.7 cm (∼19 diameters) downstream.

This Hall thruster has an extensive experimental data set[1–21] which is among the largest available. These data have been used extensively for model validation.[22–29] The experimental data from this effort are compared to simulations of the plume performed using plasma plume model DRACO. DRACO is an electrostatic particle-in-cell (PIC) code used to simulate plume of electric propulsion devices.

Due to the fundamental differences between on-orbit and vacuum facility thruster operation, this study also sought to characterize the differences in plume properties produced by various thruster and environmental conditions and to correlate these differences to various physical mechanisms. Primarily this consisted of the variation of background pressure to the extent possible within vacuum facility (∼ 3.5× nominal). Several thruster parameters (e.g. discharge voltage and current) were also varied, but these effects were more difficult to isolate.

II. Experimental Measurements

Experimental Facilities

The experimental measurements presented in this work were performed in Chamber 6 at the Air Force Research Laboratory (AFRL) Electric Propulsion Laboratory at Edwards AFB, CA. Chamber 6 is a non-magnetic stainless steel chamber with a 1.8 m diameter and 3.0 m length. It has a measured cryogenic

*Research Engineer, AFRL/PRSS, 1 Ara Rd. Edwards AFB, CA 93524, Member AIAA
†Research Engineer, AFRL/PRSS, 1 Ara Rd. Edwards AFB, CA 93524, Senior Member AIAA
‡Graduate Student, Dept. of Aerospace and Ocean Eng., Virginia Tech, Blacksburg, VA 24061, Student Member AIAA

pumping speed of 32,000 l/s on xenon. Chamber background pressure during thruster operation is approximately 5×10^{-6} Torr, corrected for xenon. Table 1 shows the nominal operating conditions for the BHT-200 200 W Hall thruster in this set of experiments. The anode current during these tests was slightly lower than usual due to the age of the thruster. A thruster at beginning of life typically has a discharge current of approximately 0.80 A. The thruster coordinate system used in this experimental study is diagrammed in Fig. 1(a).

A two-stage translation system was used to move the plasma probes relative to the thruster. A rotation stage provided angular movement. The center of rotation was lined up directly below the center of the thruster exit plane. A linear stage was stacked on top of the rotation stage to control the radial distance of the probe. Figure 1(b) depicts a schematic of the probe translation system.

Table 1. Nominal BHT-200 Operating Conditions.

Anode flow	840 μg/s (Xe)
Cathode flow	98 μg/s (Xe)
Anode potential	250 V
Anode current	0.72 A
Keeper current	0.5 A
Magnet current	1.0 A
Heater current	3.0 A

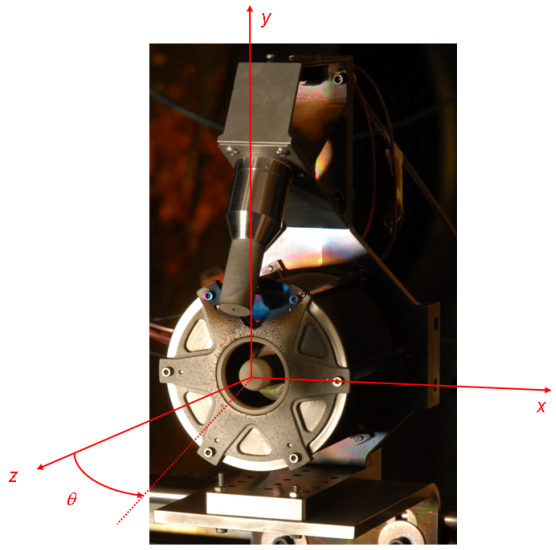

(a) Thruster coordinate system. Note: $z = 0$ is located at the exit plane.

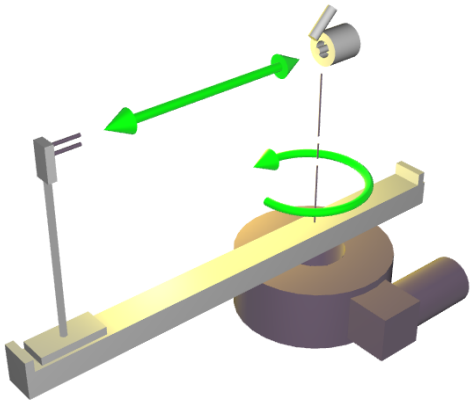

(b) The probe translation system is composed of a rotary stage for angular motion and a linear stage for radial movement.

Figure 1. Thruster coordinate system and probe translation system.

Plasma Probes

Faraday Probe

Ion current flux was measured using a guarded Faraday probe. Figure 2 shows the probe used in the experimental measurements. The electrodes were constructed from molybdenum. Ion current was collected with a disk measuring 0.312" in diameter. A concentric guard piece was used to minimize the effects of the plasma sheath on the ion current collector's effective collecting area. The guard piece was 0.885" in outer diameter. The disk and guard ring were biased to -30 V with respect to chamber ground during the

measurements so that ion saturation was achieved. The effects of secondary electron emission were assumed to be less than a few percent[30] and were neglected in the analysis of the measurements.

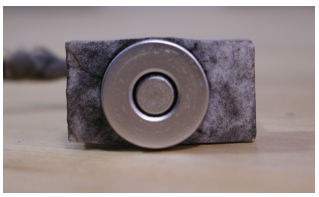

Figure 2. Faraday Probe.

Double Probe

A double Langmuir probe[31,32] was used to measure plasma density. A double probe consists of two electrodes that float with respect to the plasma. Voltage is swept between the two electrodes while current collected by the electrodes is measured. Because the mean probe potential must remain at plasma floating potential, an equal amount electron and ion current is collected by the electrodes. The main advantage of double probe is that it never draws a current from the plasma that exceeds the ion-saturation current, thus preventing excessive probe heating. Analysis of the double probe current-voltage characteristic relationship provides measurements of plasma temperature, plasma density, and Debye length.

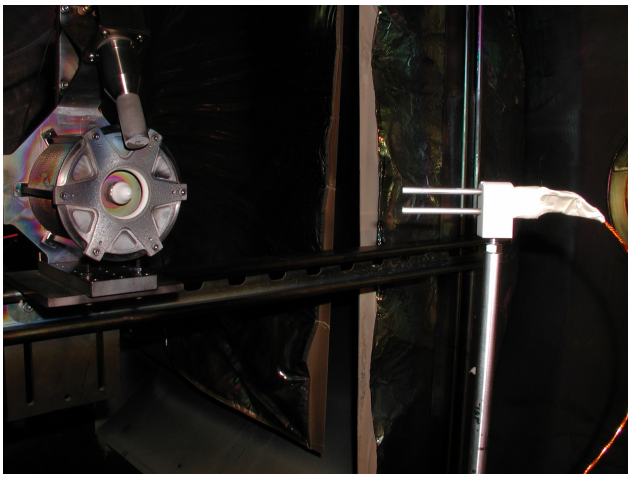

Figure 3. Double probe shown with BHT-200 thruster.

Figure 3 shows the double probe used in the present experiments. The electrodes were constructed of tungsten rod. They measured 51 mm in length with a diameter of 4 mm. They were separated by a distance of 12 mm (center to center). The probe diameter was sized large in order to ensure a high ratio of the probe diameter to the plasma sheath thickness. Keeping this ratio large ensures that surface area of the electrode is nearly as large as its effective current collecting area (taking into account plasma sheath thickness), which reduces uncertainty in the calculation of plasma density. The probe length was chosen to keep the ratio of electrode lateral surface area to tip area large. Electrode tips are prone to collecting ion current from direct impingement of the thruster plume and thus add uncertainty to collected current from the probe voltage sweep. The probe was sized so that lateral electrode area was greater than 50 times the tip area. A Keithley 2400 sourced voltage to the double probe while also measuring electrode current.

The current-voltage ($I - V$) characteristic trace for a double probe is analyzed to find ion saturation current and electron temperature. The analytical characteristic trace for electrodes with equal areas can be described as[32]

$$I = I_i \tanh\left(\frac{V}{2T_e}\right) \tag{1}$$

where I is current, I_i is ion saturation current, V is voltage, and T_e is electron temperature. In practice however, the $I-V$ trace exhibits effects from sheath expansion and plasma non-uniformities. The experimental data fits a function (adapted from Ref. 33)

$$I = I_i \tanh\left(\frac{V+V_0}{2T_e}\right) + A1\,(V+V_0) + A2 \tag{2}$$

where V_0 is a fit parameter to account for voltage offsets, $A1$ is the coefficient that accounts for sheath expansion, and the coefficient $A2$ accounts for plasma non-uniformities. A typical sample of double probe data is shown in Fig. 4.

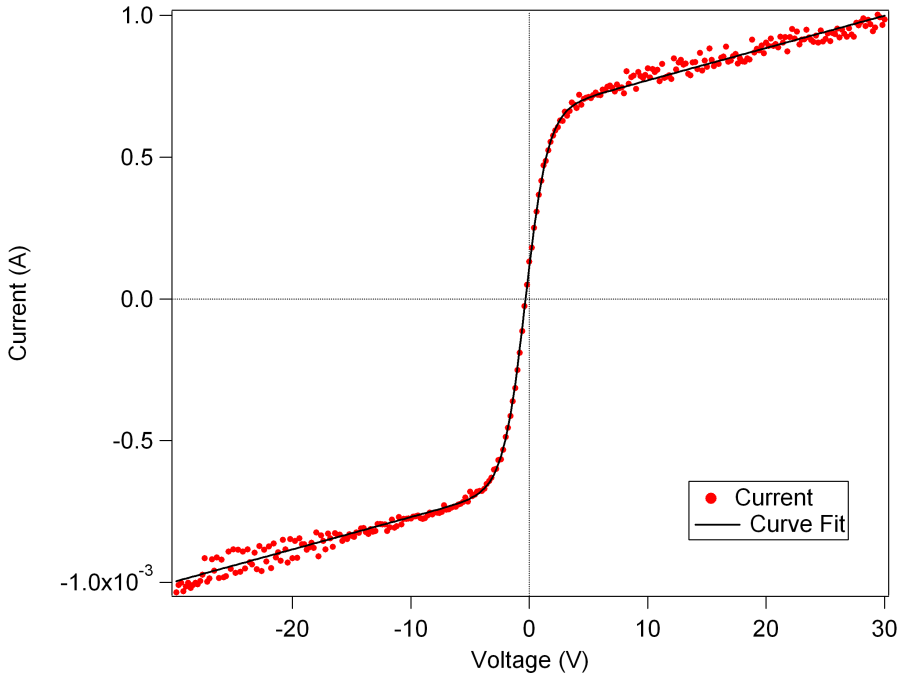

Figure 4. A typical current vs. voltage trace from the double probe. The experimental data is shown in red dots. The data was fitted with Eqn. 2. The curve fit is shown by the black line.

Analysis of the double probe data was a multi-step procedure. First, a function of the form of Eqn. 2 was fit to the data using a curve fitting routine with the commercial software program IGOR. The function fit provided values for I_{sat} and T_e. Next plasma density was calculated from the Bohm velocity approximation as

$$n_i = \frac{I_i}{Ae}\sqrt{\frac{m_i}{kT_e}} \tag{3}$$

where n_i is the plasma density, A is the collection area of the electrode, e is the elementary charge, m_i is the ion mass, and k is the Boltzmann constant. In this initial calculation, the probe surface area was considered to be collection area of the electrode. However, the actual collection area of the electrode depends on the sheath thickness. An iterative method from Ref. 34 was used to solve for both sheath thickness and plasma density.

Langmuir Probe

Several techniques were examined to measure the plasma potential in the plume of the Hall thruster. The first consisted of a 0.38 mm diameter 2% thoriated tungsten filament approximately 13 mm long heated by a DC current as shown in Fig. 5. With this technique, the probe floated near the plasma potential. These measurements provided a lower bound, approximately 1-2 T_e (empirical term where T_e is in eV), below the actual plasma potential (in volts).[35] In an attempt to improve the accuracy of the plasma potential measurements, voltage sweeps of the cold and heated probes were subtracted from one another to amplify

the knee of the $I-V$ characteristic. These data were relatively easily interpreted, but with a penalty of requiring both cold and hot $I-V$ characteristics. In addition, the lifetime of the hot filament was insufficient for extensive data sets. Upon comparison of the various techniques, it was determined that only using the cold probe $I-V$ characteristic with differentiation and a peak fit provided the ideal mix of probe lifetime and accuracy with a small computational penalty for a slightly more complex analysis. Figure 6 shows a typical $I-V$ trace, the derivative of the current with respect to voltage, and the peak fit of the current dervivative. The voltage of the derivative peak was considered to be the plasma potential. The floating potential was the current at $V=0$. As these $I-V$ characteristics were used to determine the floating and plasma potential, the electron temperature is easily derived using the Bohm criterion as[36]

$$\phi - \phi_f = \frac{kT_e}{e}\left(3.34 + 0.5\ln\left(\mu\right)\right) \tag{4}$$

where ϕ is the plasma potential, ϕ_f is the floating potential, and μ is the ion mass in multiples of the hydrogen atom mass.

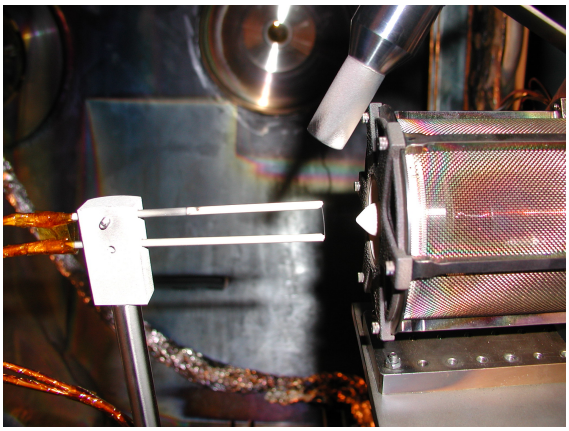

(a) The emissive probe shown with the BHT-200 thruster.

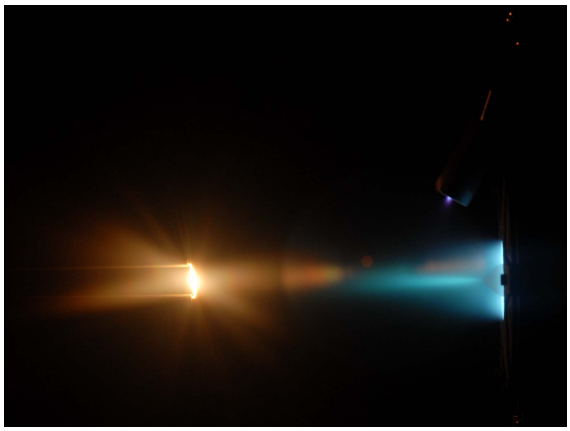

(b) Emissive probe heated during a hot $I-V$ characteristic measurement.

Figure 5. The emissive probe. Ultimately, it was most often used in a non-heated mode.

III. Experimental Results

Faraday Probe

A high resolution Faraday probe data set was taken for nominal thruster operating conditions. Data was taken from $r = 10.7$ cm to $r = 60.7$ cm in 1 cm increments. At each radius, data were taken between 0 and 180° in 1° increments. Other cases were run repeating nominal conditions and also with off-nominal operating conditions. Data for these cases were taken at radii of 15.7, 30.7, 45.7, and 60.7 cm with data from 0 to 180° in 1° increments.

The ion current flux data is shown in a logarithmic contour plot in Fig. 7 for the high resolution nominal operating condition case. The measurements indicated that the plume is highly symmetric in the $x-z$ plane as expected. Figure 8(a) shows the ion current flux for four different radii as a function of angle. The data show a localized area of high current flux at angles of approximately 70° off the thrust-axis. The current collected in these regions is thought to be from charge-exchange ions. These low-energy ions are formed from ion-neutral collisions in the plume and often travel on oblique trajectories. As the thruster plume expands radially from the acceleration channel, ion current decreases by a factor of approximately $1/r^2$. Figure 8(b) presents the ion current flux per solid angle. Presenting the data in this format allows for convenient comparison of the plume shape for various radii.

Test cases were run to reveal the effects of pressure on the population of charge-exchange ions in the oblique angles of the plume. One case was run at the nominal Chamber 6 background pressure of 4.0×10^{-6} Torr and the other case was run at a pressure of 1.4×10^{-5} Torr (pressures corrected for Xe). Note: these two cases were run with a magnet current of 0.5 A instead of the the nominal 1.0 A in order to enable a more

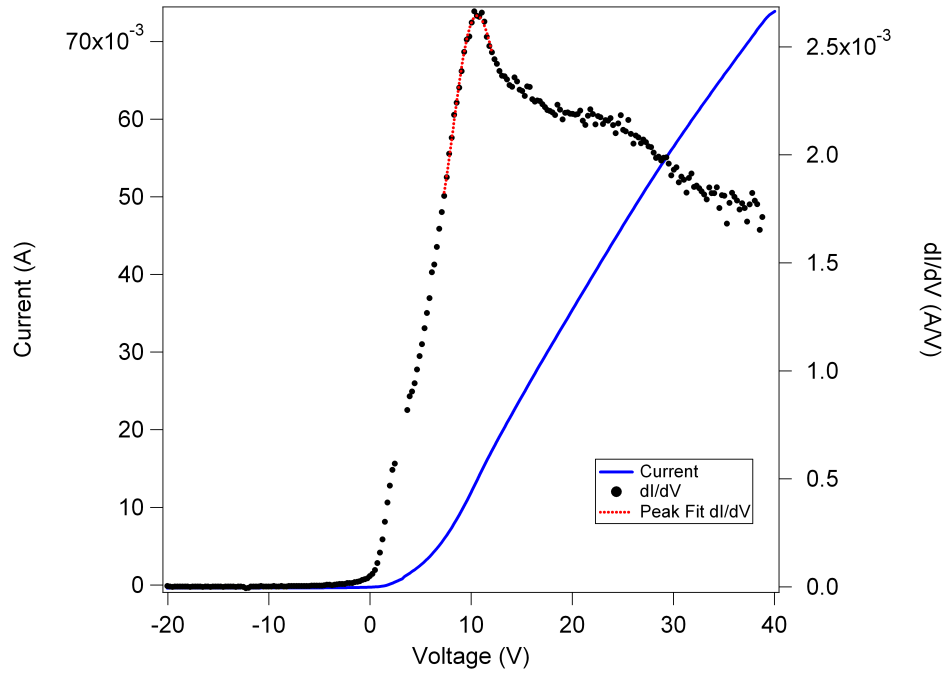

Figure 6. $I-V$ **trace for the cold emissive probe. To find plasma potential, the current trace is differentiated. A curve is fitted to the peak of the trace derivative. The plasma potential is the voltage where the derivative peak occurs. Note: A portion of the** $\mathrm{d}I/\mathrm{d}V$ **curve was discarded due to auto-ranging related defects in the current curvature from the current measuring instrument**

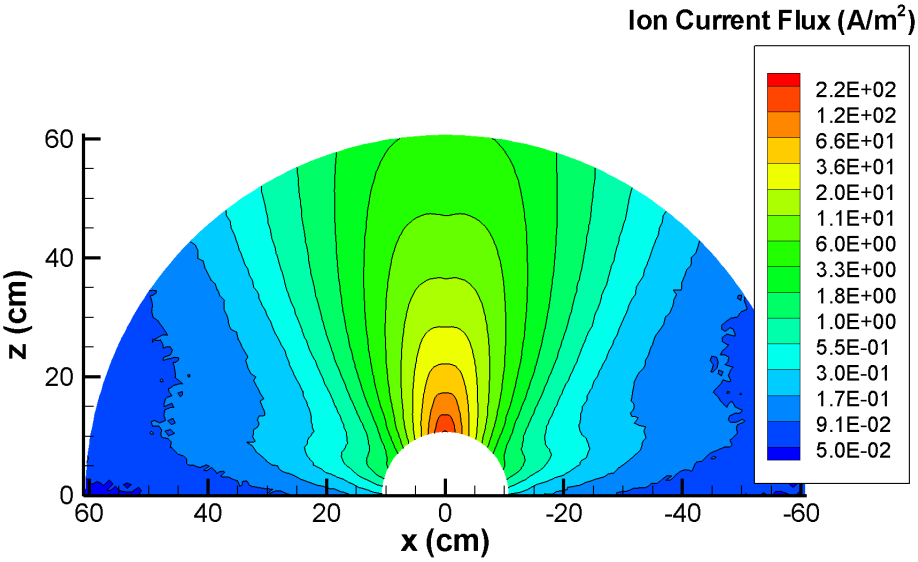

Figure 7. High resolution ion current flux data set taken for the nominal thruster operating condition.

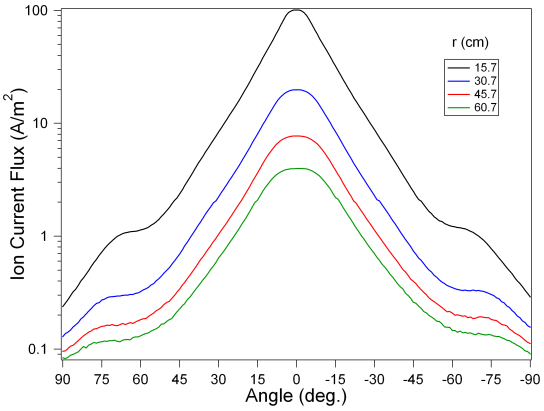

(a) Ion Current Flux (Area) vs. Angle.

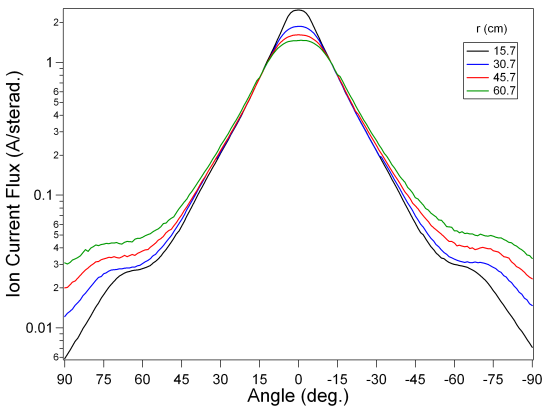

(b) Ion Current Flux (Solid Angle) vs. Angle.

Figure 8. Ion current flux at r = 15.7, 30.7, 45.7, and 60.7 cm.

stable thruster operation during the high pressure case. Figure 9(b) shows the ion current density per unit solid angle at four radii for the nominal and elevated ($\sim 3.5\times$) background pressures. This figure immediately shows several effects of plume collisions. First, it is obvious as the path length increases the ions in the plume core are deflected and the ion flux decreases. Between 15.7 and 60.7 cm, the solid angle flux drops by 50%. This increased collisionallity is demonstrated by the significant increases in the far wings ($> 45°$) of the ion current distributions also showing increases of 50%. Another interesting feature is the rise in the central core flux at all radii at higher background pressure. This result is not intuitive and the exact mechanism is unknown. It may be possible that the ion flux exiting the thruster is increased by thruster ingestion of neutrals. Alternatively, recent unpublished laser induced fluorescence xenon ion velocity measurements show that similar increases in background pressure produce a 5–10% increase in ion exit velocity. This increase in velocity appears to extend 10 cm beyond the exit plane. As a result the core flow may be better focused to some degree.

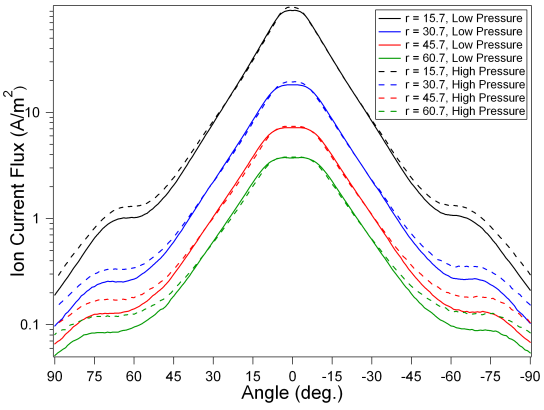

(a) Ion Current Flux (Area) vs. Angle.

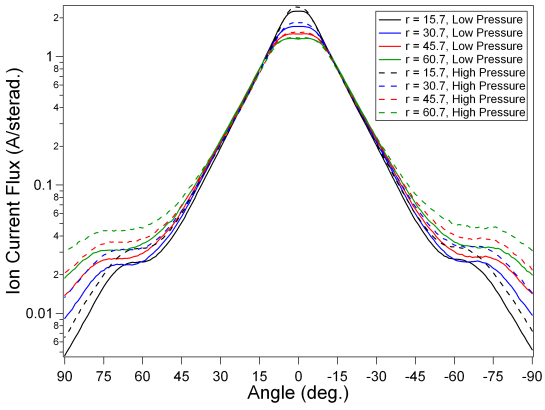

(b) Ion Current Flux (Solid Angle) vs. Angle.

Figure 9. Ion current flux at r = 15.7, 30.7, 45.7, and 60.7 cm shown for both low and high pressure cases.

A test case was run with discharge voltage of 200 V to determine the effect of discharge voltage on ion current flux. However, the difference between this case and the nominal case was actually smaller than the difference of repeated nominal condition cases. The effects of cumulative run-time on the thruster appeared to have a greater effect on ion current flux than this 50 V change in discharge voltage.

Double Probe

Double probe measurements were taken at radial distances from $r = 10.7$ to 60.7 cm in 5 cm increments and at angles from 0 to 180° in 5° increments. The relatively large size of the probe limited the spatial resolution of the measurements. The location of measurement was considered to be midpoint between the two electrode centers. Plasma density measurement for nominal thruster operating conditions are shown in Fig. 10.

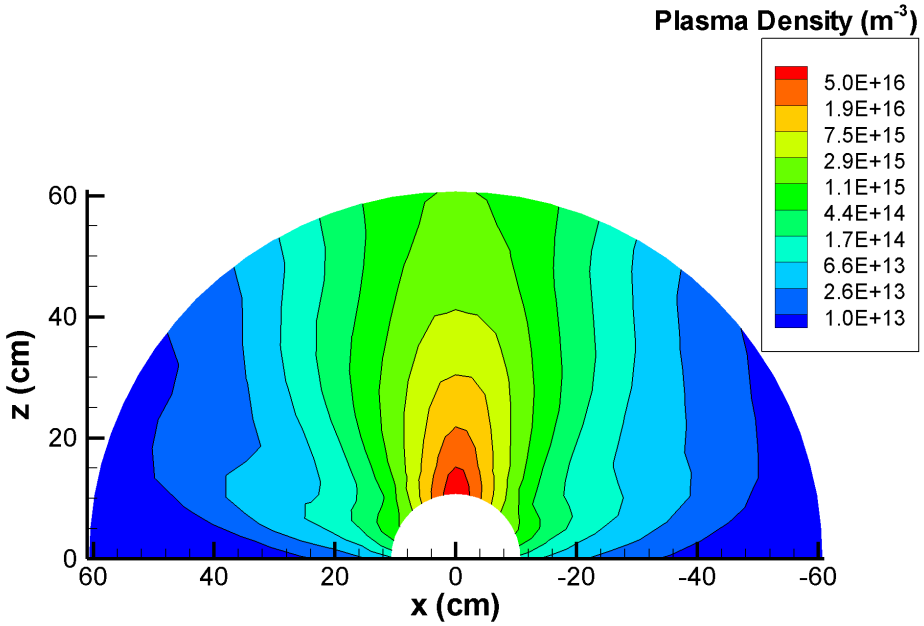

Figure 10. Plasma density as measured by the double probe for nominal thruster operating conditions.

The double probe measurements show symmetric plasma density data in the core of the plume structure. However, some asymmetry is observed at high angles with respect to the thrust axis in low density areas of the plume. This asymmetry may be due to slight misalignment of the probe or be caused by chamber effects. The measurement uncertainty is also greater in the lower density areas of the plume due to an increase in plasma sheath thickness. When compared to triple probe data from Ref. 12, these plasma density values are lower by approximately a factor of two.

Langmuir Probe

Langmuir (cold emissive probe) measurements were made throughout the plume to gather plasma potential, floating potential, and electron temperature data. For the near-plume region ($r = 1.7$ to 13.7 cm), measurements were made radially in 1 cm increments. In the far-plume region ($r = 13.7$ to 59.7 cm), measurements were spaced 2 cm apart radially. Data was taken between 0 and 180° in 5° increments. However, the angular range of data varied for values of r less than 5.7 cm. Some angles were not accessible due to the thruster geometry and some of the $I - V$ traces at the extreme angles were unusable.

Figure 11 displays the Langmuir probe data throughout the entire region of measurement. A close-up plot of the near-plume region is shown if Fig. 12. Two distinct regions of high plasma potential and electron temperature are observed a few cm directly downstream from the acceleration channel on both sides of the nose cone. This trend is not seen in electron temperature data from either the emission spectroscopy in Ref. 20 or the triple probe in Ref. 12 where T_e is highest along the thruster centerline in both cases. Even though the acceleration channel peak feature of the data does not match these other data, the temperature magnitude variation with z shows reasonable agreement with Ref. 20 and the small triple and spherical Langmuir probe measurements in Ref. 12. Hot emissive probe data from Ref. 12 taken at points 5 to 15 cm downstream show plasma potential to be a few volts lower than the present measurements, but show good overall agreement.

Floating potential measurements were the simplest data to record. These data may be useful as a subject of comparison in future modeling studies due the fact that there is little uncertainty in these measurements. However, some of the floating potential measurement results were unexpected. A region of negative floating potential was observed around $\theta = 45°$ and $r = 10$ cm. This region seemed to affect the symmetry of the rest of the plume. The cause of the negative floating data is unknown. However, it may be an effect of the chamber environment.

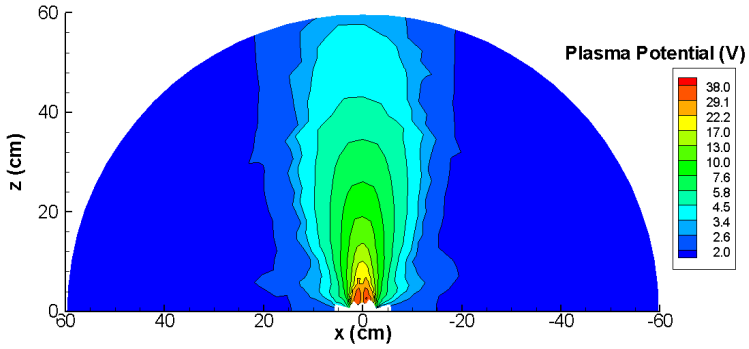

(a) Plasma potential (Note: Contour is in log scale).

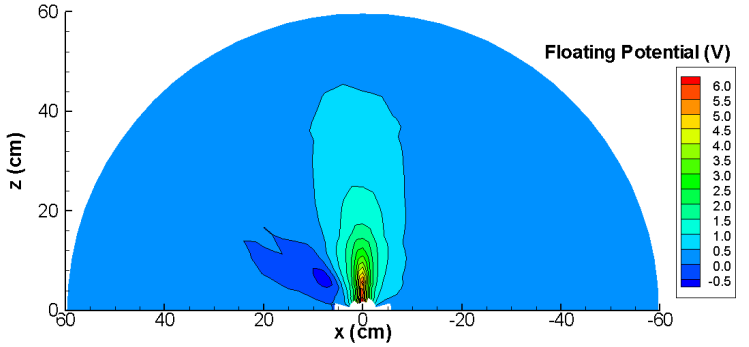

(b) Floating potential.

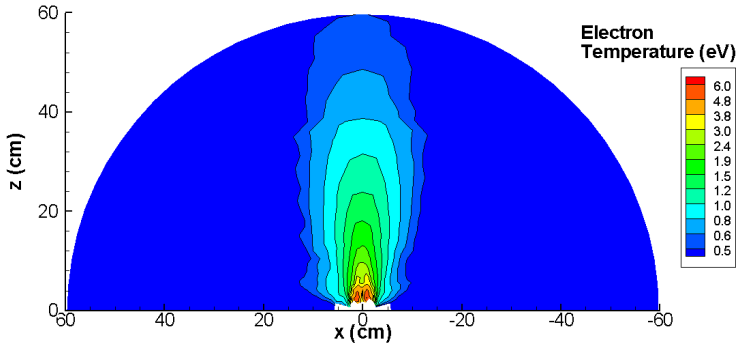

(c) Electron temperature.

Figure 11. Langmuir probe data.

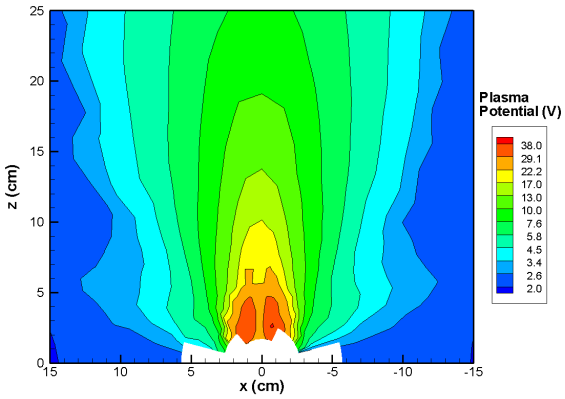

(a) Plasma Potential (Note: Contour is in log scale).

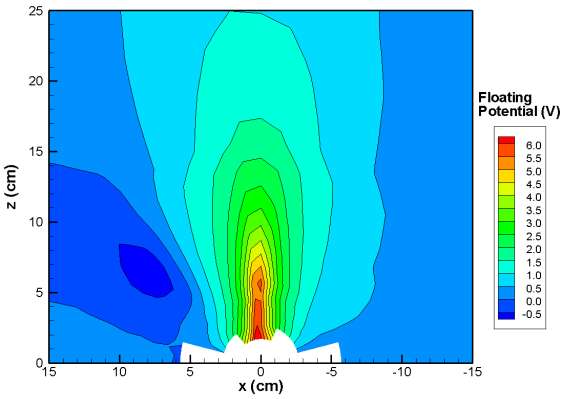

(b) Floating Potential

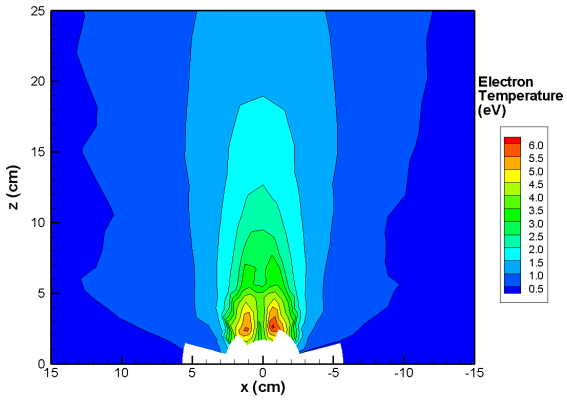

(c) Electron Temperature

Figure 12. Near-plume Langmuir probe data.

IV. Numerical Modeling

DRACO Model

The experimental data was used to validate the DRACO simulation tool. DRACO is a parallel electrostatic particle-in-cell (ES-PIC) code developed under the AFRL COLISEUM framework. DRACO operates on a rectilinear mesh which can be arbitrarily stretched in any of the three axial directions. Surface boundaries are specified by cut cells. Further overview of DRACO is available in Refs. 37 and 38.

Simulation Setup

View of the simulation setup can be seen in Fig. 13. The walls of the vacuum chamber were not included in the simulation in order to decrease mesh dimensions, and hence speed up convergence. From the simulation perspective, the primary role of the vacuum chamber is to contain the neutral particles. As shown by Spicer,[39] representation of the neutral background using discrete particles has an insignificant effect on the solution and neutrals can be modeled more efficiently as a fluid. Ion-neutral collisions were treated with the MCC method.

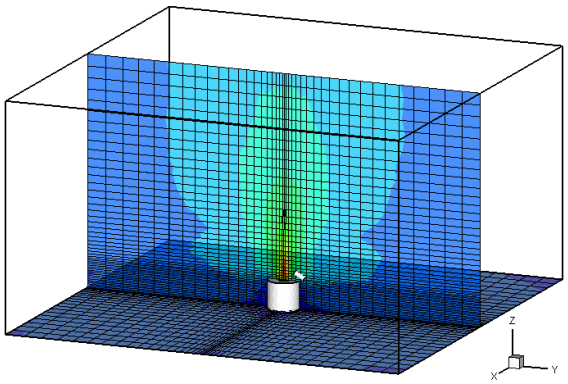

Figure 13. Simulation domain and the thruster geometry. Simulation was performed using a stretched mesh.

The thruster geometry was created using DS SolidWorks and was triangulated with Altair HyperMesh. The cathode was included in the geometry, but neutral injection from the cathode was not modeled. Plume particles were injected using the newly developed HPHall-based source, which is discussed in the following section. The simulation was performed on a single 2.8 GHz Pentium CPU with 1 Gb of RAM.

The simulation volume consisted of a stretched $40 \times 40 \times 46$ mesh. The mesh extended from 8 cm behind the thruster exit plane to 60 cm in front of the thruster. Vacuum chamber environment was approximated by an uniform background neutral density corresponding to 5×10^{-6} Torr. Plasma potential was computed from the polytropic relationship,

$$\phi = \phi_0 + kT_0 \left(\frac{\gamma}{\gamma - 1} \right) \left[(n/n_0)^{\gamma - 1} - 1 \right] \tag{5}$$

with reference values obtained by sampling experimental measurements at a location near the thruster nose cone. The values used in this simulation were $\phi_0 = 26$ V, $kT_0 = 5$ eV and $n_0 = 7.67 \times 10^{17}$ m^{-3}. These reference values can be used in conjunction with laboratory potential and density data to obtain an estimate for the polytropic γ term. The resulting map of γ, computed by inversion of Eqn. 5, can be seen in Fig. 14. Three regions are clearly visible, indicating that factors additional to density affect the temperature gradient. This dependence could not be modeled by the field solver used in this simulation, and γ was set to 1.3, which corresponds to the value seen in the low density region.

Particle Source

In the PIC method, plasma is represented by a collection of simulation macroparticles which are accelerated according to self-induced and external electromagnetic fields. The particle injection model specifies the initial condition for the velocity field, and hence it is critical to chose a source term with a good correlation to the

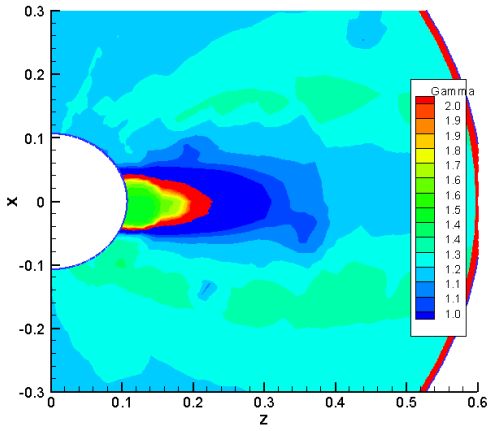

Figure 14. Polytropic γ as obtained from laboratory data. Three distinct regions are clearly visible.

flow generated by the plasma thruster. The physical mechanisms responsible for acceleration in Hall Effect Thrusters are complicated by presence of magnetic fields, sheath effects and plasma oscillations, and the velocity at the exit plane cannot be described using a simple analytical form.

Previous COLISEUM modeling efforts used a particle source based on velocity profiles obtained experimentally using laser induced fluorescence (LIF).[10] Radial variation in mass flux was determined by interpolation of mid-field Faraday probe data to the thruster exit plane. The primary issue with this source, FLUX_R_VZ_VR, was related to the velocity sampling method. The available LIF data set was limited to the three primary velocity components: axial, radial and azimuthal. Since these components are located in an orthogonal space, no information was available about their correlation, and each component had to be sampled independently. This limitation resulted in production of particles with excessive amounts of kinetic energy.

Instead, it was necessary to develop a source capable of sampling particles with correlated velocities. The input data set could be obtained through an extensive laboratory effort by sampling the velocity field at multiple angular locations. However, a more cost effective option was to use a simulation tool to model the acceleration processes inside the Hall thruster. The simulation presented in this paper was performed using HPHall,[40] a 2D axi-symmetric code developed under a collaboration of AFOSR and MIT. A detailed sensitivity study of HPHall as applied to the BHT-200-X3 thruster was presented in Ref. 29. The input conditions corresponded to the "low mobility, near cathode" case. As discussed in Ref. 29, this case produced the best agreement with LIF measurements at the exit plane.

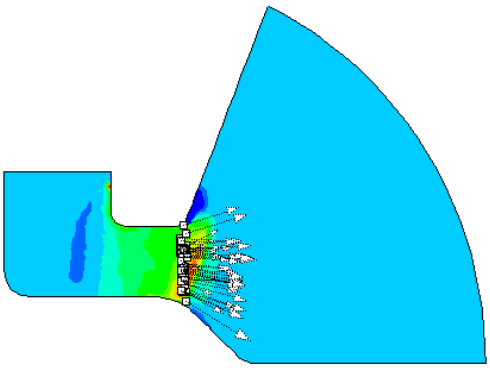

Figure 15. Computational domain for the HPHall simulation showing the sampling region and several representative velocity vectors.

Input data for the plume simulation was obtained by sampling particles crossing the exit plane. The velocity components along with the radial position were stored in a data file corresponding to the particle

charge. This data was then used to inject singly and doubly-charged ions into the DRACO simulation. Neutral particles were loaded as a drifting Maxwellian. Transformation to the 3D coordinates was performed using the following set of equations:

$$\vec{x}^i = P\vec{x}^p + x_0 \tag{6}$$
$$\vec{v}^i = P\vec{v}^p \tag{7}$$

where

$$\vec{p}^p = r\hat{p}_1 \tag{8}$$
$$\vec{v}^p = v_r\hat{p}_1 + v_\theta\hat{p}_2 + v_z\hat{p}_3 \tag{9}$$

and

$$P = \begin{bmatrix} (\tau_{1x}\cos\theta - \tau_{2x}\sin\theta) & (\tau_{1x}\sin\theta + \tau_{2x}\cos\theta) & n_x \\ (\tau_{1y}\cos\theta - \tau_{2y}\sin\theta) & (\tau_{1y}\sin\theta + \tau_{2y}\cos\theta) & n_y \\ (\tau_{1z}\cos\theta - \tau_{2z}\sin\theta) & (\tau_{1z}\sin\theta + \tau_{2z}\cos\theta) & n_z \end{bmatrix} \tag{10}$$

Here $\hat{\tau}_1$ and $\hat{\tau}_2$ indicate two orthogonal vectors in the plane of the thruster, and $\hat{n}$ is the thruster normal direction. The particle selection was performed in a random order using a high period random number generator.[41]

An improvement in correlation with the experimental data can be clearly seen in figure 16. This plot shows the Faraday probe data, previously presented in Fig. 7, compared to results obtained using several COLISEUM sources. The MAXSTREAM results were obtained by injecting the ions as a drifting Maxwellian. A non-physical temperature had to be used to obtain the beam divergence seen in laboratory. The FLUX_R_VZ_VR source was described previously. Although this source is based on experimental data, the resulting beam is too collimated, with a poor agreement in the charge exchange wing. An excellent agreement is achieved with the HPHALL source in both plume and low density region. The only significant discrepancy can be seen within 5° of the centerline where the simulation over-predicts the collected current.

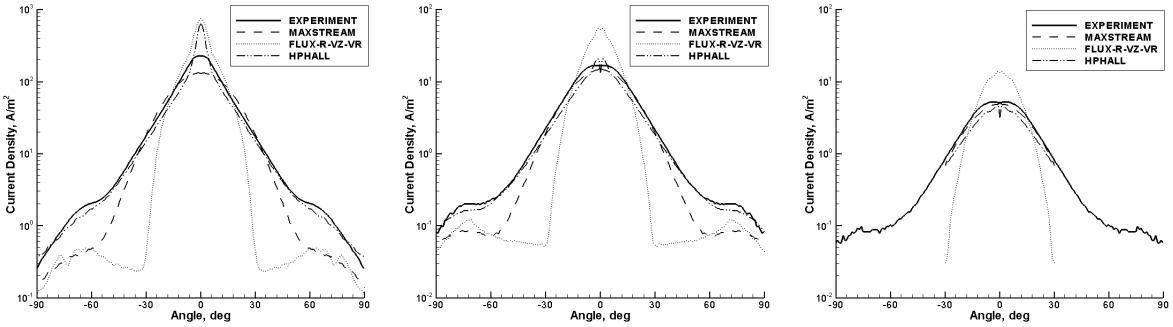

(a) $r = 10$ cm (b) $r = 30$ cm (c) $r = 50$ cm

Figure 16. Comparison of experimental and simulation current density at several axial points for three COLISEUM sources.

V. Modeling Results

Contour plots of potential, number density and polytropic temperature are shown in Fig. 17. The white contour lines correspond to the experimental data. The experimental potential ranges from 38.7 V near the thruster to 1.8 V in the wings. In the region swept by the probes, the numerical results instead vary from 27.7 to 1.8 V. Similar trend is seen in the number density data. Although the agreement is good in the main plume, the simulation overestimates the wing density by a factor of 4. The simulation data ranges from 9.5×10^{16} to 9.1×10^{12} m^{-3}, while the experimental data shows values between 1.0×10^{17} and 2.0×10^{12}m^{-3}. Finally, the value of polytropic temperature obtained from the simulation ranges from 0.28 to 5.3 eV, while the experimental data show values in the range of 0.27 and 6.0 eV.

This data is further analyzed in the XY plots of Fig 18. These plots show simulation and experimental values of potential, density and temperature along three radial sweeps. Radius of 0 cm corresponds to the

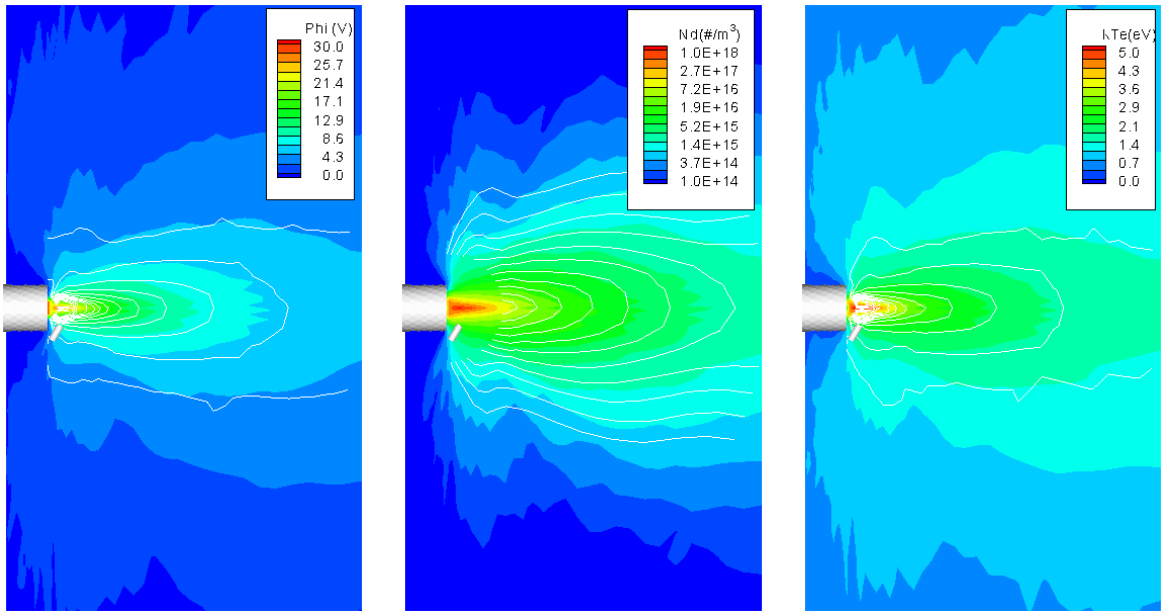

(a) phi (b) n_d (c) kTe

Figure 17. Contour plots of simulation potential, plasma density and electron temperature. White contour lines indicate experimental data.

exit plane. The data is plotted at 10, 30, and 50 cm, except in the case of number density, for which the 10 cm data was not available. Solid lines correspond to the experimental data, while the dashed lines show results obtained by the simulation. The plots indicate very good agreement at 10 cm. All three plume properties exhibit decay rates analogous to the experimental rates. Small discrepancy occurs at high angles, where the simulation data plateaus faster than expected. A very good agreement is seen in magnitudes as well, except for the case of polytropic temperature. This discrepancy is likely due to the choice of reference values, and the limitations of the potential solver used in this simulation.

The agreement becomes worse as the distance from the thruster is increased. While trends seen in the temperature plot agree with the lab data, the discrepancy is increased for potential and density. The simulation predicts the correct potential in the wing, but overestimates the centerline potential. Conversely, the centerline ion density matches the experimental values, but the wing density is over-estimated. At 50 cm, the simulation over-predicts the centerline potential, while underestimating the wing potential. An acceptable agreement is seen in the density data, but the decay is not as rapid as suggested by the experiment.

Particle velocities were also compared to data from the E×B probe at 60 cm. The comparison can be seen in Fig. 19. A virtual probe was implemented in DRACO to sample particles crossing a 60 cm hemisphere centered at the exit plane. Sampling region was set to $\pm 5°$ off the nominal angle. A 5° acceptance angle was implemented by rejecting particles for which $\hat{r} \cdot \hat{v} > \cos(5°)$, where $\hat{r}$ is the vector from the thruster nose cone to the point on the hemisphere, and $\hat{v}$ is the particle velocity vector. A very good agreement is seen within the first 20° of the centerline. At higher angles, the simulation velocity traces become dominated by the slow moving CEX ions. The experimental data, on the other hand, shows a significant primary beam population up to 50°. The experimental data becomes noisy at the larger angles, but a trace of the primary beam ions can be seen up to 80°. This discrepancy is likely due to lack of momentum transfer collisions in the simulation.

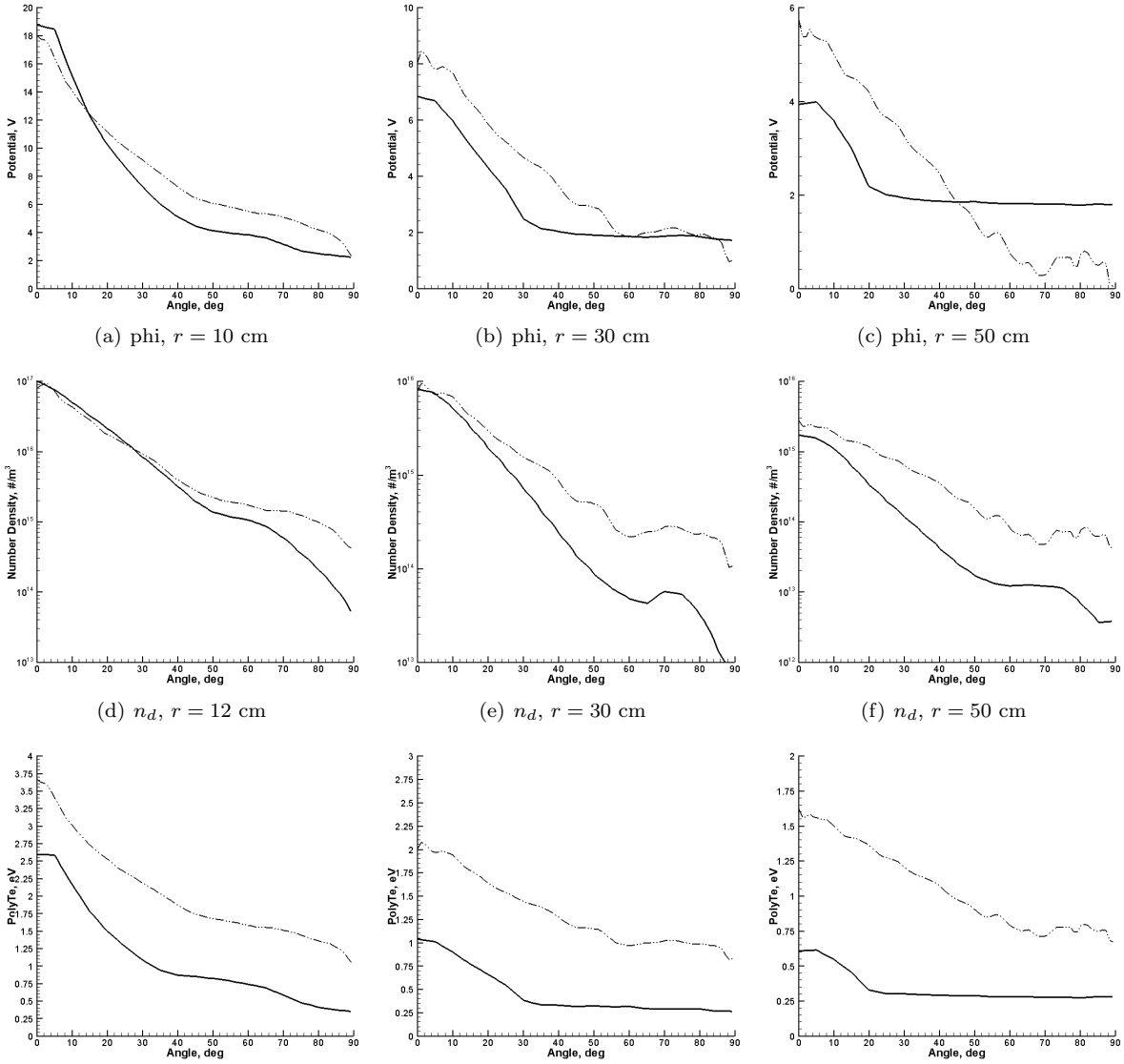

(a) phi, $r = 10$ cm (b) phi, $r = 30$ cm (c) phi, $r = 50$ cm

(d) n_d, $r = 12$ cm (e) n_d, $r = 30$ cm (f) n_d, $r = 50$ cm

(g) kTe, $r = 10$ cm (h) kTe, $r = 30$ cm (i) kTe, $r = 50$ cm

Figure 18. Radial plots of plasma potential, ion density and polytropic temperature at three different axial positions. Density is plotted at 12 cm due to lack of experimental data at 10 cm. Experimental data is shown by the solid line.

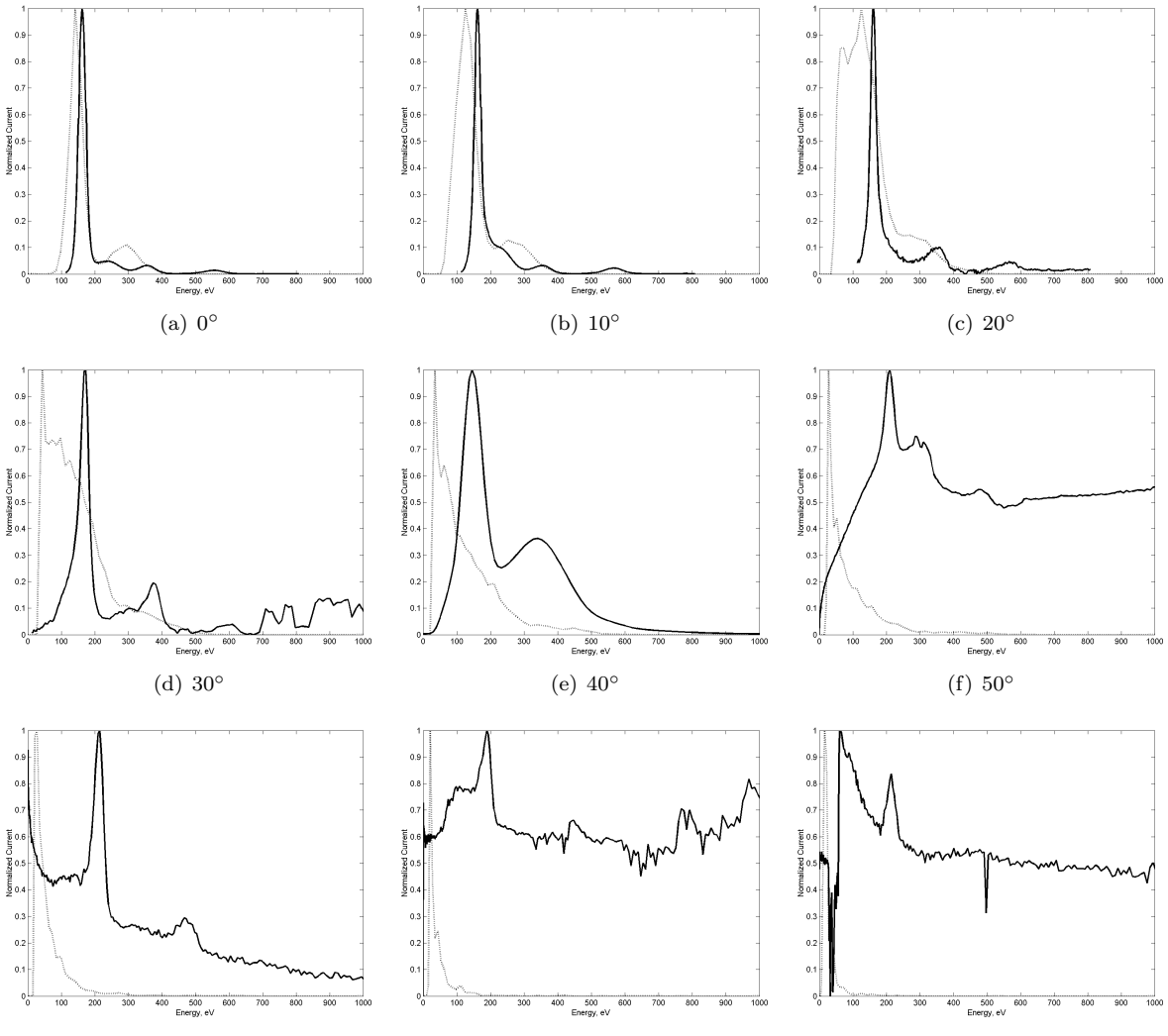

(a) 0° (b) 10° (c) 20°

(d) 30° (e) 40° (f) 50°

(g) 60° (h) 70° (i) 80°

Figure 19. Comparison of ion energies at various angles at $r = 60$ cm. Experimental data is shown by the solid line.

VI. Conclusions and Future Work

An extensive set of experimental measurements has characterized the plume of the BHT-200 thruster. Ion current flux, plasma density, plasma potential, floating potential, and electron temperature measurements have been made between the near-plume and 60 cm downstream of the exit plane. Faraday probe measurements run at 3.5× nominal chamber background pressure showed an increase in charge exchange ion at oblique angles in the plume when compared with measurements at nominal pressure. A slight increase in ion core-flux was also noticed for the high pressure case. Electron temperature and plasma potential data showed peak value regions that corresponded to the acceleration channel. These peak locations were not observed in measurements from other studies. In the future more analysis will be performed on data from off-nominal thruster conditions to study the effects of discharge voltage and magnet current on the plume.

The experimental data was used to validate the DRACO simulation code. The simulation was performed by assuming a polytropic dependence of temperature on density and the Boltzmann relationship for electrons. Ions were injected according to correlated velocity distribution obtained by a simulation of the Hall thruster with the HPHall code. An excellent agreement was obtained with the Faraday probe data. The potential, density and temperature results were also in a good agreement, with some discrepancies at high angles and increased distance from the exit plane. Particle energies exhibit agreement with experimental measurements in the main plume, but the simulation did not predict the population of primary beam ions at large angles from the centerline seen in E×B measurements. Additional sensitivity study is needed to investigate the effect of particle collisions, potential solver and source injection model on the simulation results. Future modeling studies will analyze the effects of background pressure on the plume characteristics.

References

[1]Beal, B. E., Gallimore, A. D., Haas, J. M., and Hargus, Jr., W. A., "Plasma Properties in the Plume of a Hall Thruster Cluster," *Journal of Propulsion and Power*, Vol. 20, No. 6, November-December 2004, pp. 985–991.

[2]Hargus, Jr., W. A. and Reed, G., "The Air Force Clustered Hall Thruster Program," *38th AIAA/ASME/SAE/ASEE Joint Propulsion Conference*, Indianapolis, IN, 2002, AIAA-2002-3678.

[3]Hargus, Jr., W. A. and Pote, B., "Examination of a Hall Thruster Start Transient," *38th AIAA/ASME/SAE/ASEE Joint Propulsion Conference*, Indianapolis, IN, 2002, AIAA-2002-3956.

[4]Beal, B., Gallimore, A., and Hargus, Jr., W. A., "Preliminary Plume Characterization of a Low-Power Hall Thruster Cluster," *38th AIAA/ASME/SAE/ASEE Joint Propulsion Conference*, Indianapolis, IN, 2002, AIAA-2002-4251.

[5]Parcos, A., *Plume Experiment on the Space Shuttle*, Master's thesis, MIT, Cambridge, MA, 2002.

[6]Hargus, Jr., W. A., "Interactions within a Cluster of Low Power Hall Thrusters," *28th International Electric Propulsion Conference*, Toulouse, France, 2003, IEPC-2003-030.

[7]Azziz, Y. and Martinez-Sanchez, M., "Plasma Measurements on a 200-Watt Hall Thruster Plume," *28th International Electric Propulsion Conference*, Toulouse, France, 2003, IEPC-2003-140.

[8]Beal, B., Gallimore, A., and Hargus, Jr., W. A., "The Effects of Clustering Multiple Hall Thrusters on Plasma Plume Properties," *39th AIAA/ASME/SAE/ASEE Joint Propulsion Conference*, Huntsville, AL, 2003, AIAA-2003-5155.

[9]Hargus, Jr., W. A. and Cappelli, M. A., "Interactions within a Cluster of Low Power Hall Thrusters," *39th AIAA/ASME/SAE/ASEE Joint Propulsion Conference*, Huntsville, AL, 2003, AIAA-2003-5006.

[10]Hargus, Jr., W. A. and Charles, C. S., "Near Exit Plane Velocity Field of a 200 W Hall Thruster," *39th AIAA/ASME/SAE/ASEE Joint Propulsion Conference*, Huntsville, AL, 2003, AIAA-2003-5154.

[11]Azziz, Y., *Development and Plasma Measurements on a 200-Watt Hall Thruster Plume*, Master's thesis, MIT, Cambridge, MA, 2003.

[12]Beal, B. E., *Clustering of Hall Effect Thrusters for High-Power Electric Propulsion Applications*, Ph.D. thesis, University of Michigan, Ann Arbor, MI, 2004.

[13]Cappelli, M., Hermann, W., Kodiak, M., Gascon, N., and Hargus, Jr., W., "A 90 GHz Phase-Bridge Interferometer for Plasma Density Measurements in the Near Field of a Hall Thruster," *40th AIAA/ASME/SAE/ASEE Joint Propulsion Conference*, Fort Lauderdale, FL, 2004, AIAA-2004-3775.

[14]Cappelli, M. and Hargus, Jr., W., "Images of Ground State Xenon Density in the Near Field of Low Power Hall Thruster," *40th AIAA/ASME/SAE/ASEE Joint Propulsion Conference*, Fort Lauderdale, FL, 2004, AIAA-2004-4120.

[15]Hargus, Jr., W. and Straffaccia, J., "Optical Boron Nitride Insulator Erosion Characterization of a 200 W Xenon Hall Thruster," *41th AIAA/ASME/SAE/ASEE Joint Propulsion Conference*, Tucson, AZ, 2005, AIAA-2005-3529.

[16]Beal, B., Gallimore, A., and Hargus, Jr., W. A., "The Effects of Cathode Configuration on Hall Thruster Cluster Plume Properties," *41st AIAA/ASME/SAE/ASEE Joint Propulsion Conference*, Tucson, AZ, 2003, AIAA-2005-3678.

[17]Hargus, Jr., W., "Laser-Induced Fluorescence of Neutral Xenon in the Near Field of a 200 W Hall Thruster," *41th AIAA/ASME/SAE/ASEE Joint Propulsion Conference*, Tucson, AZ, 2005, AIAA-2005-4400.

[18]Ekholm, J. and Hargus, Jr., W., "E×B Measurements of a 200 W Xenon Hall Thruster," *41th AIAA/ASME/SAE/ASEE Joint Propulsion Conference*, Tucson, AZ, 2005, AIAA-2005-4405.

[19]Hargus, Jr., W. and Nakles, M., "Evolution of the Ion Velocity Distribution in the Near Field of the BHT-200-X3 Hall Thruster," *42nd AIAA/ASME/SAE/ASEE Joint Propulsion Conference*, Sacramento, CA, 2006, AIAA-2006-4991.

[20]Matlock, T., Hargus, Jr., W., Larson, C., and Nakles, M., "Inversion Method for Reconstructing Hall Thruster Plume Parameters from Optical Measurements," *43rd AIAA/ASME/SAE/ASEE Joint Propulsion Conference*, Cincinnati, OH, 2007, AIAA-2007-5303.

[21]Matlock, T., Hargus, Jr., W., and Larson, C., "Thermographic Characterization and Comparison of 200 W and 600 W Hall Thrusters," *43rd AIAA/ASME/SAE/ASEE Joint Propulsion Conference*, Cincinnati, OH, 2007, AIAA-2007-5241.

[22]Cheng, S., *Computational Modeling of a Hall Thruster Plasma Plume in a Vacuum Tank*, Master's thesis, MIT, Cambridge, MA, 2002.

[23]Santi, M., *Thruster Plume Simulation Using a Hybrid-PIC Algorithm*, Master's thesis, MIT, Cambridge, MA, 2003.

[24]Fife, J., Gibbons, M., Hargus, Jr., W., VanGilder, D., Kirtley, D., and Johnson, L., "3-D Computation of Surface Sputtering and Redeposition Due to Hall Thruster Plumes," *28th International Electric Propulsion Conference*, Toulouse, France, 2003, IEPC-2003-0136.

[25]Celik, M., Santi, M., Cheng, S., Martinez-Sanchez, M., and Peraire, J., "Hybrid-PIC Simulation of a Hall Thruster Plume on an Unstructured Grid with DSMC Collisions," *28th International Electric Propulsion Conference*, Toulouse, France, 2003, IEPC-2003-134.

[26]Santi, M., Cheng, S., Celik, M., Martinez-Sanchez, M., and Peraire, J., "Further Development and Preliminary Results of the AQUILA Hall Thruster Plume Model," *39th AIAA/ASME/SAE/ASEE Joint Propulsion Conference*, Huntsville, AL, 2003, AIAA-2003-4873.

[27]Cheng, S., Santi, M., Celik, M., Martinez-Sanchez, M., and Peraire, J., "Hybrid PIC-DSMC simulation of a Hall thruster plume on unstructured grids," *Computer Physics Communications*, , No. 164, 2004, pp. 73–79.

[28]Boyd, I. and Yim, J. T., "Modeling of the near field plume of a Hall thruster," *Journal of Applied Physics*, Vol. 95, No. 9, May 2004, pp. 4575–4584.

[29]Nakles, M., Hargus, Jr., W., and VanGilder, D., "Comparison of Numerical and Experimental Near-Field Ion Velocity Distributions of the BHT-200-X3 Hall Thruster," *42nd AIAA/ASME/SAE/ASEE Joint Propulsion Conference*, Sacramento, CA, 2006, AIAA-2006-4479.

[30]Brown, S. C., *Basic Data of Plasma Physics*, American Institute of Physics Press, New York, 1994.

[31]Hutchinson, I., *Principles of Plasma Diagnostics*, Cambridge University Press, New York, 1994.

[32]Liberman, M. A. and Lichtenberg, A. J., *Principles of Plasma Dicharges and Materials Processing*, John Wiley & Sons, Inc., New York, 1994.

[33]Smith, B. and Overzet, L., "Improvements to the floating double probe for timeresolved measurements in pulsed rf plasmas," *Review of Scientific Instruments*, Vol. 69, No. 3, March 1998, pp. 1372.

[34]Haas, J. M., *Low-Perturbation Interrogation of the Internal and Near-Field Plasma Structure of a Hall Thruster Using a High-Speed Probe Positioning System*, Ph.D. thesis, University of Michigan, Ann Arbor, MI, 2001.

[35]Dorf, L., Raitses, Y., and Fisch, N., "Electrostatic probe apparatus for measurements in the near-anode region of Hall thrusters," *Review of Scientific Instruments*, Vol. 75, No. 5, May 2004, pp. 1255–1260.

[36]Ruzic, D. N., *Electron Probes for Low Temperature Plasmas*, AVS Press, New York, 1994.

[37]Brieda, L., Pierru, J., Kafafy, R., and Wang, J., "Development of the DRACO Code for Modeling Electric Propulsion Plume Interactions," *40th AIAA/ASME/SAE/ASEE Joint Propulsion Conference*, Fort Lauderdale, FL, 2004, AIAA-2004-3533.

[38]Spicer, R. L., *Validation of the DRACO Particle-in-Cell Code using Busek 200W Hall Thruster Experimental Data*, Master's thesis, Virginia Tech, Blacksburg, VA, 2007.

[39]Spicer, R. L., Wang, J., and Brieda, L., "Modeling Particle Collisions with DRACO Electric Propulsion Simulation Package," *42nd AIAA/ASME/SAE/ASEE Joint Propulsion Conference*, Sacramento, CA, 2006, AIAA-2006-5025.

[40]Fife, J. M., *Hybrid-PIC Modeling and Electrostatic Probe Survey of Hall Thrusters*, Ph.D. thesis, Massachusetts Institute of Technology, Cambridge, MA, 1998.

[41]Matsumoto, M. and Nishimura, T., "A 623-dimensionally equidistributed uniform pseudorandom number generator," *ACM Trans. on Modeling and Computer Simulation*, Vol. 8, No. 1, January 1998, pp. 3–30.